Effects of macromolecular crowding on protein folding and aggregation studied by density functional theory: Dynamics

Akira R. Kinjo[1,*] and Shoji Takada[1,2,†]
[1]*PRESTO, Japan Science and Technology Corporation, Kobe University, Kobe 657-8501, Japan*
[2]*Department of Chemistry, Faculty of Science, Kobe University, Kobe 657-8501, Japan*
(Received 21 March 2002; revised manuscript received 28 August 2002; published 7 November 2002)

Inside the living cell is inherently crowded with proteins and other macromolecules. Thus, it is indispensable to take into account various interactions between the protein and other macromolecules for thorough understanding of protein functions in cellular contexts. Here we focus on the excluded volume interaction imposed on the protein by surrounding macromolecules or ''crowding agents.'' We have presented a theoretical framework for describing equilibrium properties of proteins in crowded solutions [A. R. Kinjo and S. Takada, Phys. Rev. E (to be published)]. In the present paper, we extend the theory to describe nonequilibrium properties of proteins in crowded solutions. Dynamics simulations exhibit qualitatively different morphologies depending on the aggregating conditions, and it was found that macromolecular crowding accelerates the onset of aggregation while stabilizing the native protein in the quasiuniform phase before the onset of aggregation. It is also observed, however, that the aggregation may be kinetically inhibited in highly crowded conditions. The effects of crowding on folding and unfolding of proteins are also examined, and the results suggest that fast folding is an important factor in preventing aggregation of denatured proteins.

DOI: 10.1103/PhysRevE.66.051902 PACS number(s): 87.15.Nn, 87.15.Aa

I. INTRODUCTION

Unlike in typical biochemical experiments in which the proteins of interest are purified and diluted, the living cell is inherently crowded with a wide variety of other proteins and macromolecules which generally occupy 20–30 % of the total cell volume [1]. It is natural to expect that miscellaneous interactions present in such crowded conditions may alter physical, biochemical, and even physiological properties of the protein of interest [2]. Among all the complex interactions between proteins and macromolecules, the excluded volume effect is of prominent importance because it is always present as long as molecules exist. The effects imposed by the excluded volume of macromolecules are called ''macromolecular crowding'' effects [2–6] and those macromolecules that impose such effects are termed ''crowding agents'' [5]. Among a wide variety of phenomena affected by macromolecular crowding, we focus on crowding effects on protein stability, folding, and aggregation in this paper.

Not only static properties but also dynamic aspects of macromolecular crowding and aggregation are also of much interest because formation of aggregates such as inclusion bodies and amyloid fibrils is always a dynamical process. Recently, it has been suggested that transient aggregates during amyloid fibril formation may be inherently toxic to the cell, regardless of whether or not the final amyloid fibrils are toxic [7]. The experimental measurement of the crowding effect on the rate of amyloid formation is also reported, indicating that crowding accelerates amyloid formation [8]. There are also theoretical studies of aggregation kinetics under the influence of crowding agents [8,9]. Although some theories can describe the kinetics of aggregation semiquantitatively or even quantitatively, they predefine the structure of aggregates and only the growth rate of aggregates can be tracked. Recently, molecular simulation studies on the competition between protein folding and aggregation have also been performed [10–12]. Molecular simulations have advantages in that they can provide detailed pictures of protein conformational changes upon folding and/or aggregation. However, the number of proteins and other macromolecules that can be handled in a simulation is limited, whereas aggregation typically involves quite a large number of molecules. To complement simple kinetic theories and detailed molecular simulations, there is a need for another theoretical framework that can track the morphological evolution as well as the growth rate of aggregates consisting of a large number of proteins.

In our previous paper [13], we presented a density functional theory that describes a system of proteins and crowding agents at equilibrium, and showed that crowding effects on protein stability and aggregation can be treated in a unified framework. Two main results obtained there are that, as the bulk density of the crowding agent increases, aggregation of denatured proteins is enhanced and the native protein is increasingly stabilized unless aggregation occurs [13]. Here we extend the theory to treat nonequilibrium phenomena such as aggregation dynamics. The method used here is based on a dynamic density functional theory [14] which is widely used in simulations of phase separation dynamics of, for example, polymer melts [15,16]. With this extension, it has become possible to see dynamic aspects of crowding effects on protein stability, folding, and aggregation in a unified framework.

The paper is organized as follows. In Sec. II, we briefly summarize the free energy density functional presented previously [13], and then formulate a set of equations that describe the dynamics of the density fields of the protein and

*Electronic address: akinjo@theory.chem.sci.kobe-u.ac.jp
†Electronic address: stakada@kobe-u.ac.jp

crowding agent. The results of dynamics simulations are presented in Sec. III, showing morphological variations of transient aggregates and crowding effects on aggregation as well as on folding and unfolding. Section IV tries to relate the simulation results with the crowding effects in the cell and some experimental observations. The conclusion is given in Sec. V.

II. THEORY AND MODELING

A. Density functional

The free energy density functional that describes the system of proteins and crowding agents was introduced in our preceding paper [13]. We briefly review it here.

First, the system we consider consists of two chemical species: one protein species (denoted by P) and one crowding agent species (C). But the protein can be either native (N) or denatured (D). Therefore, there are actually three physical species: N, D, and C. Each of the three species is characterized by an intrinsic free energy η_α ($\alpha=N,D,C$).

Next, we assume the following bare interaction potential ($u_{\alpha,\beta}$; $\alpha,\beta=N,D,C$) between two molecules:

$$u_{\alpha,\beta}(r)=\begin{cases}\infty & (r\leqslant R_\alpha+R_\beta),\\ \epsilon_{\alpha,\beta} & [R_\alpha+R_\beta<r\leqslant 3(R_\alpha+R_\beta)],\\ 0 & [r>3(R_\alpha+R_\beta)],\end{cases} \tag{1}$$

from which the effective interaction potential $u^{\mathrm{eff}}_{\alpha,\beta}$ is defined as [17]

$$u^{\mathrm{eff}}_{\alpha,\beta}(|\mathbf{r}|)=T(1-e^{-u_{\alpha,\beta}(|\mathbf{r}|)/T}). \tag{2}$$

Throughout this paper, we always set $\epsilon_{\alpha,\beta}=0$ for all $\alpha,\beta=N,D,C$ except for $\epsilon_{D,D}$. Since denatured proteins are, in general, prone to attract each other due to exposed hydrophobic side chains and hydrogen-bonding groups, $\epsilon_{D,D}$ is set to some negative value.

The system is represented by the density fields of the native protein, denatured protein, and the crowding agent: $\phi^N(\mathbf{r})$, $\phi^D(\mathbf{r})$, and $\phi^C(\mathbf{r})$, respectively. The solvent density $\phi^S(\mathbf{r})$ is indirectly defined by $\phi^S=\rho_0-\Sigma_\alpha\phi^\alpha$ where the summation is over $\alpha=N,D$, and C, and ρ_0 is the total bulk density of the system. Assuming that the effective interaction $u^{\mathrm{eff}}_{\alpha,\beta}$ is short ranged, the free energy functional is given by

$$F[\{\phi^\alpha(\mathbf{r})\}]=F_i+F_n, \tag{3}$$

where F_i is the ideal part,

$$F_i[\{\phi^\alpha(\mathbf{r})\}]=\int d\mathbf{r}\left[\sum_\alpha\{\eta_\alpha\phi^\alpha+T\phi^\alpha\ln\phi^\alpha\}+T\phi^S\ln\phi^S\right], \tag{4}$$

and F_n is the nonideal part,

$$F_n[\{\phi^\alpha(\mathbf{r})\}]=\frac{1}{2}\int d\mathbf{r}\sum_{\alpha,\beta}[U_{\alpha,\beta}\phi^\alpha\phi^\beta-V_{\alpha,\beta}\nabla\phi^\alpha\cdot\nabla\phi^\beta]. \tag{5}$$

Here we have defined a set of interaction parameters,

$$U_{\alpha,\beta}=\int d\mathbf{s}u^{\mathrm{eff}}_{\alpha,\beta}(|\mathbf{s}|), \tag{6}$$

$$V_{\alpha,\beta}=\frac{1}{4d}\int d\mathbf{s}|\mathbf{s}|^2u^{\mathrm{eff}}_{\alpha,\beta}(|\mathbf{s}|), \tag{7}$$

where d is the spatial dimension (i.e., $d=3$). The local chemical potential $\mu_\alpha(\mathbf{r})$ is defined as a functional derivative of the free energy F with respect to $\phi^\alpha(\mathbf{r})$,

$$\mu_\alpha(\mathbf{r})=\frac{\delta F}{\delta\phi^\alpha(\mathbf{r})}=\eta_\alpha+T\ln\left(\frac{\phi^\alpha(\mathbf{r})}{\rho_0-\sum_\beta\phi^\beta(\mathbf{r})}\right)+W_\alpha(\mathbf{r}), \tag{8}$$

where the last term $W_\alpha(\mathbf{r})\equiv(U_{\alpha,\beta}+V_{\alpha,\beta}\nabla^2)\phi^\beta(\mathbf{r})$ may be regarded as the potential of mean force for the species α.

B. Dynamics

The dynamics of the system consists of two different processes: diffusion and folding-unfolding reactions. Therefore, we assume that the following diffusion-reaction equations describe the dynamics of the system:

$$\frac{\partial\phi^N(\mathbf{r})}{\partial t}=-\nabla\cdot\mathbf{J}^N(\mathbf{r})-k_u(\mathbf{r})\phi^N(\mathbf{r})+k_f(\mathbf{r})\phi^D(\mathbf{r}), \tag{9a}$$

$$\frac{\partial\phi^D(\mathbf{r})}{\partial t}=-\nabla\cdot\mathbf{J}^D(\mathbf{r})+k_u(\mathbf{r})\phi^N(\mathbf{r})-k_f(\mathbf{r})\phi^D(\mathbf{r}), \tag{9b}$$

$$\frac{\partial\phi^C(\mathbf{r})}{\partial t}=-\nabla\cdot\mathbf{J}^C(\mathbf{r}), \tag{9c}$$

where $\mathbf{J}^\alpha(\mathbf{r})$ is the flux of the species α, and $k_u(\mathbf{r})$ and $k_f(\mathbf{r})$ are site-dependent unfolding and folding transition rates, respectively. Equations (9) are essentially the equations of continuity for the conserved variables $\phi^N(\mathbf{r})+\phi^D(\mathbf{r})$ and $\phi^C(\mathbf{r})$.

The functional form of the flux $\mathbf{J}^\alpha$ is derived heuristically from Fick's law. According to Fick's law, the flux in an ideal (dilute) solution is given by

$$\mathbf{J}^\alpha(\mathbf{r})=-D^\alpha\nabla\phi^\alpha(\mathbf{r}), \tag{10}$$

where D^α is a diffusion constant. The crowded solution is not ideal, however, and macromolecular interactions cannot be neglected. Therefore we replace the density $\phi^\alpha(\mathbf{r})$ on the right-hand side of Eq. (10) with the effective density or thermodynamic activity $a_\alpha(\mathbf{r})\equiv\exp[\mu_\alpha(\mathbf{r})/T]$. Furthermore, since the diffusion at a site will be influenced by the crowdedness of the site (the more crowded the site, the slower the diffusion there), we require that the flux is also proportional to the square of the vacancy (or solvent density) of the site, $\phi^S(\mathbf{r})$. Finally, the flux term becomes

$$\mathbf{J}^{\alpha}(\mathbf{r}) = -D^{\alpha}\{\phi^{S}(\mathbf{r})\}^{2}\nabla a_{\alpha}(\mathbf{r}) = -D^{\alpha}\{\phi^{S}(\mathbf{r})\}^{2}\nabla e^{\mu_{\alpha}(\mathbf{r})/T}. \tag{11}$$

In the limit of infinite dilution ($\phi^{\alpha}\to 0$ for all $\alpha = N,D,C$), Eq. (11) reduces to the ordinary Fick's law, Eq. (10).

The transition rates of folding and unfolding vary over sites due to stabilization or destabilization by interactions with nearby molecules. Therefore it is necessary to define site-dependent folding and unfolding transition rates. First we assume a two-state kinetics of folding and unfolding and introduce the intrinsic free energy of the transition state, η_{TS}. According to the transition state theory, the unfolding and folding rate constants (k_u^0 and k_f^0, respectively) in a dilute protein solution are given by

$$k_u^0 = \nu_0 \exp[-(\eta_{TS} - \eta_N)/T], \tag{12}$$

$$k_f^0 = \nu_0 \exp[-(\eta_{TS} - \eta_D)/T], \tag{13}$$

where ν_0 is the attempt frequency. When interactions between molecules cannot be neglected, the rate constants become site dependent. We assume that the potential of the mean force, $W_{TS}(\mathbf{r})$, for the transition state protein is a linear combination of those for the native and denatured proteins:

$$W_{TS}(\mathbf{r}) = \omega W_N(\mathbf{r}) + (1-\omega) W_D(\mathbf{r}), \tag{14}$$

where $\omega \in [0,1]$ is a weight constant. Experimental values of Tanford's β_T [18] suggest that $\omega = 0.8$ is a reasonable value which we always use in the following. The site-dependent unfolding and folding rate constants [$k_u(\mathbf{r})$ and $k_f(\mathbf{r})$, respectively] are given by

$$k_u(\mathbf{r}) = k_u^0 \exp[-\{W_{TS}(\mathbf{r}) - W_N(\mathbf{r})\}/T], \tag{15}$$

$$k_f(\mathbf{r}) = k_f^0 \exp[-\{W_{TS}(\mathbf{r}) - W_D(\mathbf{r})\}/T]. \tag{16}$$

The reaction terms in Eq. (9a) can be rearranged as

$$\begin{aligned}\left(\frac{\partial \phi^N(\mathbf{r})}{\partial t}\right)_{\text{reaction}} &= -k_u(\mathbf{r})\phi^N(\mathbf{r}) + k_f(\mathbf{r})\phi^D(\mathbf{r}) \\ &= \nu_0 \phi^S(\mathbf{r}) e^{-\{\eta_{TS} + W_{TS}(\mathbf{r})\}/T} \\ &\quad \times (e^{\mu_D(\mathbf{r})/T} - e^{\mu_N(\mathbf{r})/T}).\end{aligned} \tag{17}$$

The reaction terms in Eq. (9b) can be rearranged in the same way, and give the negative of Eq. (17).

With the above choice of dynamics, it can be shown that the free energy is a decreasing function of time,

$$\begin{aligned}\frac{dF}{dt} &= \sum_{\alpha} \int d\mathbf{r} \frac{\delta F}{\delta \phi^{\alpha}} \frac{\partial \phi^{\alpha}}{\partial t} = \sum_{\alpha} \int d\mathbf{r} \mu_{\alpha} \frac{\partial \phi^{\alpha}}{\partial t} \\ &= -\sum_{\alpha} D^{\alpha} \int d\mathbf{r} \frac{(\phi^S)^2 e^{\mu_{\alpha}/T}}{T} |\nabla \mu_{\alpha}|^2 \\ &\quad - \nu_0 \int d\mathbf{r} \phi^S e^{-\{\eta_{TS} + W_{TS}\}/T} (\mu_N - \mu_D)(e^{\mu_N/T} - e^{\mu_D/T}) \\ &\leqslant 0.\end{aligned} \tag{18}$$

C. Numerics

1. Physical scales

We describe the physical scales of the system treated, although they have been described in the previous paper [13]. The unit of energy is defined as the folding temperature in dilute solution, which is ~ 3 kJ/mol. In all the simulations below, we set $T=1$; hence $\eta_N = \eta_D$ holds. For simplicity, we set $\eta_N = \eta_D = 0$. The intrinsic free energy of the crowding agent does not play any role in the present model; hence we set $\eta_C = 0$. These values are always used below. The intrinsic free energy of the transition state protein is set as $\eta_{TS} = 1$ or $\eta_{TS} = 5$. The former value corresponds to fast-folding proteins and is used in most of the calculations, while the latter value represents proteins which fold (and unfold) more slowly. The unit length is taken as approximately 10 nm, so that the radii of the molecules are ~ 0.1 unit length. The experimentally measured radius of gyration of the native state of the IgG binding domain of streptococcal protein L (62 amino acid residues) is 1.65 nm and that of the denatured state (denatured by GdmCl) is ~ 2.6 nm [18]. Hence $R_D \sim 1.5 R_N$. In all the calculations below, we set the radius of the native protein to 0.4 unit length and that of the denatured one to 0.6. In order to keep the volume fraction of the denatured protein in a unit volume less than unity, we set $\rho_0 = 1$. In the following numerical simulations, the linear system size is set to 64 unit length.

2. Discretization scheme

The set of partial differential equations, Eq. (9), are discretized by the line method so that the spatial dimension of the system is composed of $32\times 32\times 32$ lattice sites with the lattice constant $h = 64/32 = 2$. The periodic boundary condition is always imposed in all directions. The diffusion terms in Eq. (9) are discretized by applying central finite differencing twice. Setting $\mathbf{r} = (x,y,z)$, the discretization in the x direction reads

$$\begin{aligned}&\frac{\partial}{\partial x}[\phi^S(\mathbf{r})]^2 \frac{\partial}{\partial x} e^{\mu_{\alpha}(\mathbf{r})/T} \\ &\quad \to \frac{1}{h^2}\left\{\left[\left(\phi^S\left(x+\frac{h}{2},y,z\right)\right]^2 \{e^{\mu_{\alpha}(x+h,y,z)/T} - e^{\mu_{\alpha}(x,y,z)/T}\}\right.\right. \\ &\qquad \left.\left. - \left[\phi^S\left(x-\frac{h}{2},y,z\right)\right]^2 \{e^{\mu_{\alpha}(x,y,z)/T} - e^{\mu_{\alpha}(x-h,y,z)/T}\}\right\},\end{aligned} \tag{19}$$

where $[\phi^S(x \pm h/2,y,z)]^2$ is calculated as the geometric mean:

$$[\phi^S(x \pm h/2,y,z)]^2 = \phi^S(x \pm h,y,z)\phi^S(x,y,z). \tag{20}$$

The discretized diffusion term for the lattice site $\mathbf{r}_i$ becomes

$$\begin{aligned}\left(\frac{\partial \phi^{\alpha}(\mathbf{r}_i)}{\partial t}\right)_{\text{diffusion}} &= \frac{1}{h^2} D^{\alpha} {\sum_j}' \phi^S(\mathbf{r}_i)\phi^S(\mathbf{r}_j) \\ &\quad \times (e^{\mu_{\alpha}(\mathbf{r}_j)/T} - e^{\mu_{\alpha}(\mathbf{r}_i)/T}).\end{aligned} \tag{21}$$

The summation (Σ') is taken over the neighboring sites with appropriate weighting factors:

$$\sum_j{}' = w_1 \sum_{j \in n_1} + w_2 \sum_{j \in n_2} + w_3 \sum_{j \in n_3} . \tag{22}$$

where n_1, n_2, and n_3 are the set of nearest neighbor, next-nearest neighbor, and next-next-nearest neighbor lattice sites, respectively. As in the preceding paper [13], the weighting factors are adopted from Ref. [19], that is, $w_1 = 0.294\,726$, $w_2 = 0.235\,425$, and $w_3 = 0.175\,818$. The discretized diffusion term here is the same as that introduced by Gouyet [20] for describing order-disorder dynamics of alloys.

The diffusion constant D^α may, in general, depend on species, but here we use $D^\alpha = 0.1$ for all species. The attempt frequency ν_0 of folding-unfolding transition rates is also set to 0.1.

The spatial discretization of the diffusion-reaction Eq. (9) produces a stiff set of ordinary differential equations with respect to time t. Numerical integration of these ordinary equations was performed using an explicit Runge-Kutta-Chebyshev method of second order. We used the ROCK2 code developed by Abdulle and Medovikov [21].

D. Analysis of dynamics simulations

The time evolution of the system is monitored in terms of the change in free energy, the relative fraction of the native protein ($f_N = \langle \phi^N \rangle / \langle \phi^N + \phi^D \rangle$), and the relative spatial deviation s of the native protein density [$s_N = \sqrt{\langle (\phi^N - \langle \phi^N \rangle)^2 \rangle} / \langle \phi^N \rangle$]. The angular brackets $\langle\ \rangle$ denote averaging over the system. The morphology of denatured aggregates can be visualized by the isosurfaces of the density field of the denatured protein, $\phi^D(\mathbf{r})$. In order to quantitatively examine morphological characteristics of aggregates, we make use of the characteristic length of the system defined in terms of the structure factor. First, defining the Fourier transform of $\phi^P(\mathbf{r}) = \phi^N(\mathbf{r}) + \phi^D(\mathbf{r})$ as

$$\hat{\phi}^P(\mathbf{k}) = \int d\mathbf{r} \phi^P(\mathbf{r}) e^{\sqrt{-1}\mathbf{k}\cdot\mathbf{r}}, \tag{23}$$

the structure factor $S(\mathbf{k})$ is given by

$$S(\mathbf{k}) = \langle \hat{\phi}^P(\mathbf{k}) \hat{\phi}^P(-\mathbf{k}) \rangle_{\text{noise}} . \tag{24}$$

The brackets $\langle\ \rangle_{\text{noise}}$ on the RHS of Eq. (24) means averaging operation over different initial noise fields. In practice, we use the discrete Fourier transform for $\hat{\phi}^P(\mathbf{k})$ so that the values of $\mathbf{k}$ are discrete. Following Shinozaki and Oono [22], the characteristic length scale is defined as $2\pi/\langle k \rangle$ where

$$\langle k \rangle = \frac{\sum_{\mathbf{k} \neq \mathbf{0}} |\mathbf{k}|^{-1} S(\mathbf{k})}{\sum_{\mathbf{k} \neq \mathbf{0}} |\mathbf{k}|^{-2} S(\mathbf{k})} . \tag{25}$$

Note that the mode $\mathbf{k} = \mathbf{0}$ is excluded in this definition of $\langle k \rangle$ so that $2\pi/\langle k \rangle$ does not diverge when the system is completely uniform.

III. RESULTS

A. Morphological variations of aggregation processes

We first performed several tentative simulations with small bulk density of the crowding agent $\rho_C = 0.05$ in order to determine the range of the interaction parameter $\epsilon_{D,D}$ that can cause the aggregation of the denatured protein. In all the following calculations, we set the bulk number density of the protein $\rho_P = 0.1$, and all $\epsilon_{\alpha,\beta} = 0$ except for $\epsilon_{D,D}$. The initial density fields were set quasiuniform such that $\phi^N(\mathbf{r}) = 0.5\rho_P[1 + \xi^N(\mathbf{r})]$, $\phi^D(\mathbf{r}) = 0.5\rho_P[1 + \xi^D(\mathbf{r})]$, and $\phi^C(\mathbf{r}) = \rho_C[1 + \xi^C(\mathbf{r})]$ where $\xi^\alpha(\mathbf{r})$ are uniform random fields in the range $[-0.1, 0.1]$. Additional corrections were made to enforce the conditions that $\langle \phi^N + \phi^D \rangle = \rho_P$, $\langle \phi^C \rangle = \rho_C$, and $0 < \phi^A(\mathbf{r}) < \rho_0$ for $A = N, D, C$, and S. Each simulation consists of ten runs with the same parameters but with different initial random fields. The radii of the molecules were set as $R_N = 0.4$, $R_D = 0.6$, and $R_C = 0.4$, and the intrinsic free energy of the transition state protein is given by $\eta_{TS} = 1$.

Two morphologically different regimes of aggregation of the denatured protein were found depending on the value of $\epsilon_{D,D}$ (Fig. 1).

Figures 1(a)–1(c) correspond to the simulation with $\epsilon_{D,D} = -0.11$ which is the minimum negative value for the aggregation to occur (i.e., for $\epsilon_{D,D} > -0.11$, aggregation was not observed). In this simulation, a small number of the denatured aggregates of quasispherical shapes form after some latent time [Fig. 1(a), $t = 6 \times 10^3$], which then grows rapidly. As the simulation proceeds, larger aggregates grow larger whereas smaller ones become even smaller and eventually vanish [Fig. 1(b)]. One large aggregate survives at the final stage [Fig. 1(c)]. This case with $\epsilon_{D,D} = -0.11$ may correspond to a nucleation regime of aggregation, and we call it the nucleationlike regime in the following.

Figures 1(d)–1(f) show the morphological evolution in the simulation with $\epsilon_{D,D} = -0.2$ which makes the system more liable to aggregate than the previous simulation. This case corresponds to the spinodal decomposition regime. In this simulation, a large number of small aggregates form immediately [Fig. 1(d), $t = 3 \times 10^2$]. These small aggregates rapidly grow and coalesce to form large spongelike aggregates [Fig. 1(e)], which then contract and split into smaller pieces [Fig. 1(f)]. During the course of evolution, the aggregates of complex shapes become of simpler and more spherical forms. The transient spongelike aggregates [Fig. 1(e)] are only loosely connected in the sense that the density of the denatured protein does not change significantly between inside and outside the aggregates. The aggregates at later stages [Fig. 1(f)] are denser. These differences of the aggregates in Figs. 1(e) and 1(f) are clearly seen in Fig. 2 where the distribution of the denatured proteins in the spongelike aggregates [Fig. 2(a)] is in sharp contrast to that in aggregates at a later stage [Fig. 2(b)].

Next we turn to the time evolution of physical quantities. Figure 3 shows the time evolution of characteristic length

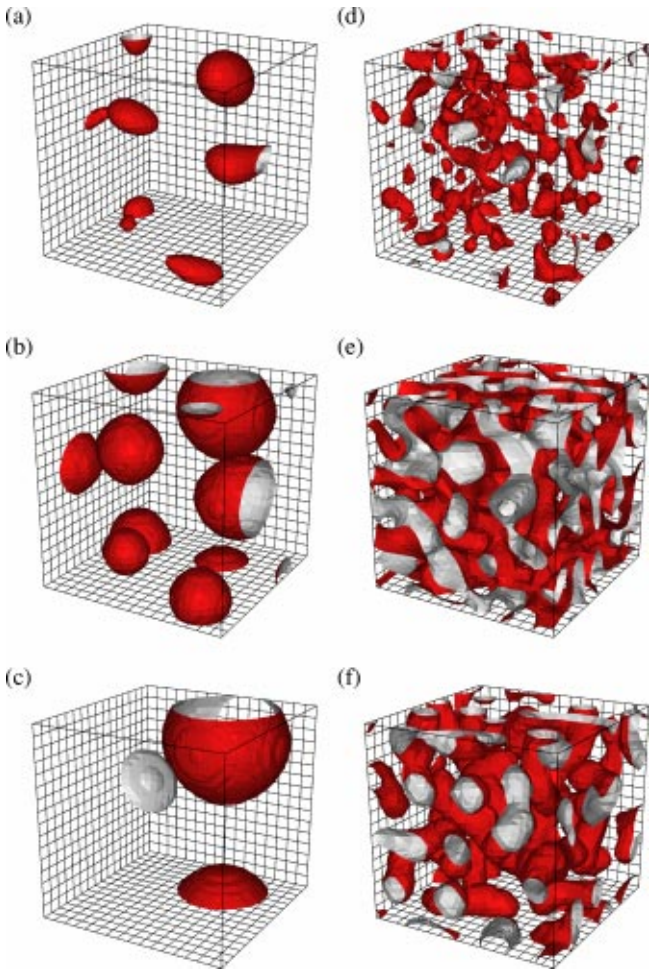

FIG. 1. Morphological evolution of the aggregates of the denatured proteins represented by the isosurface of $\phi^D(\mathbf{r})=0.1$. (a)–(c) correspond to $\epsilon_{D,D}=-0.11$, and (d)–(f) to $\epsilon_{D,D}=-0.2$. The bulk protein density ρ_P is set to 0.1 in both cases. Times: (a) $t=6\times10^3$, (b) $t=1\times10^5$, (c) $t=5\times10^5$, (d) $t=3\times10^2$, (e) $t=1\times10^3$, and (f) $t=1\times10^5$.

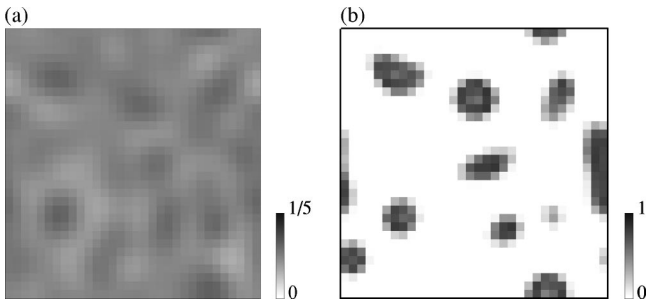

FIG. 2. Cross sections of the system with $\rho_P=0.1$ and $\epsilon_{D,D}=-0.2$. The density field of the denatured protein $\phi^D(\mathbf{r})$ is shown. (a) and (b) correspond to $t=1\times10^3$ [cf. Fig. 1(e)] and $t=1\times10^5$ [cf. Fig. 1(f)], respectively. Note that the gray scale ranges from 0 to 0.2 in (a), and from 0 to 1 in (b).

$2\pi/\langle k\rangle$, free energy, fraction of the native protein $f_N=\langle\phi^N\rangle/\rho_P$, and relative spatial deviation of the native protein density $s_N=\sqrt{\langle(\phi^N-\langle\phi^N\rangle)^2\rangle}/\langle\phi^N\rangle$.

The characteristic length $2\pi/\langle k\rangle$ in the nucleationlike regime [Fig. 3(a), dark line] initially increases until $t\sim1000$ when it starts to decrease until $t\sim5000$. The relative spatial deviation of the native protein density s_N [Fig. 3(d)] indicates that aggregates begin to form at $t\sim5000$ so that the sudden drop in $2\pi/\langle k\rangle$ and its subsequent increase correspond to the embryonic and growing aggregates, respectively, whereas the initial increase in $2\pi/\langle k\rangle$ may correspond to smoothing of the initial random fluctuations. The time evolution of $2\pi/\langle k\rangle$ in the spinodal decomposition regime [Fig. 3(a), light line] is rather modest compared to that in the nucleationlike one. After passing the initial hill around $t\sim100$, $2\pi/\langle k\rangle$ increases very slowly. Even after $t=10^6$, it reaches only less than 20 (unit length). This extremely slow aggregation process may be attributed to the strong interaction between the denatured proteins $\epsilon_{D,D}$ which hinders the diffusion of proteins to form larger aggregates. In the nucleationlike regime with $\epsilon_{D,D}=-0.11$, the free energy stays

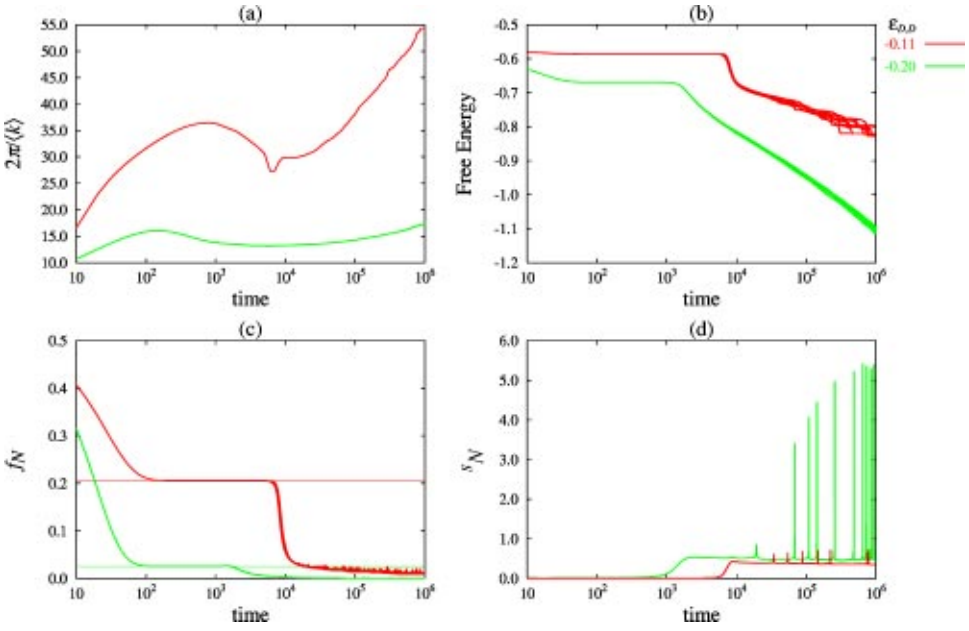

FIG. 3. Time evolution of (a) characteristic length scale $2\pi/\langle k\rangle$, (b) free energy, (c) fraction of the native protein, (d) relative spatial deviation of the native protein density s_N. In (b) and (c), ten trajectories with different initial random fields are shown for each case, whereas (d) focuses on one trajectory. Horizontal narrow lines in (c) are the equilibrium values of f_N in the uniform system.

nearly fixed until the onset of aggregation at $t \sim 10^4$ [Fig. 3(b)]. The free energy rapidly drops when initial aggregates grow larger, but the rate of decrease becomes slow after a short period of time. The effect of initial random fields appears at very late stages of aggregation, but it does not influence the latent time for the onset of aggregation. Although the free energy stays constant in the beginning, the native fraction f_N drops immediately until it reaches a plateau at $t \sim 100$ [Fig. 3(c)] where it stays at $f_N \sim 0.2$. Then at the onset of aggregation f_N sharply decreases. It is found that the value of f_N at its plateau [Fig. 3(c)] is almost identical to the value of f_N at equilibrium in the uniform phase [Fig. 3(c), narrow line] which can be calculated from the self-consistent equations presented in the preceding paper [13].

In the spinodal decomposition regime, immediate decrease in the free energy [Fig. 3(b)] is accompanied by the appearance of small aggregates [Fig. 1(d)] in early stages of aggregation process. When those small aggregates grow and the spongelike aggregates are formed [Fig. 1(e)], the free energy stays almost constant. The free energy begins to decrease again at time $t \sim 1000$, when the spongelike aggregates become denser and begin to split. The initial decrease in f_N [Fig. 3(c)] continues even after the free energy has reached the plateau [Fig. 3(b)]. Nevertheless it reaches a plateau at $t \sim 100$ with $f_N \approx 0.025$ which is also almost identical to the value at equilibrium in the uniform phase [Fig. 3(c), narrow line]. This plateau again corresponds to the spongelike aggregates [Fig. 1(e)]. The second decrease in f_N seems to be synchronized with that in the free energy [Fig. 3(b)]. In this regime, the influence of initial random fields is negligible until late stages.

In Fig. 3(d), we see a number of sharp spikes in the spatial deviation of ϕ^N, s_N. Visual inspection suggests that these spikes are associated with extinction of small denatured aggregates. Figure 4 shows a series of cross sections when a denatured aggregate vanishes in the case of the nucleationlike regime ($\epsilon_{D,D} = -0.11$) corresponding to Figs. 1(a)–1(c).

The native protein density $\phi^N(\mathbf{r})$ is indeed very low in the denatured aggregates [Fig. 4(a)]. When a denatured aggregate vanishes at a site, $\phi^N(\mathbf{r})$ increases at that site [Fig. 4(b)]. But this increase in $\phi^N(\mathbf{r})$ is only a temporary one and the density fields $\phi^N(\mathbf{r})$ and $\phi^D(\mathbf{r})$ around the site where the vanished aggregate was located rapidly reorganize to become uniform [Fig. 4(c)]. Similar behaviors are also observed in the spinodal decomposition regime ($\epsilon_{D,D} = -0.2$).

In both the nucleationlike and spinodal decomposition regimes, the effect of the initial random fields on the aggregation process is not significant except for late stages. This was also true in other simulations presented below. Therefore, the time evolution of physical quantities such as free energy, native fraction (f_N), and relative spatial deviation (s_N) is shown only for one trajectory for clarity.

B. Crowding effects on aggregation process

We now examine effects of macromolecular crowding on the process of aggregation by performing dynamics simulations for different values of the bulk crowding agent density ρ_C. The intrinsic free energy of the transition state protein is set to $\eta_{TS} = 1$ in this section.

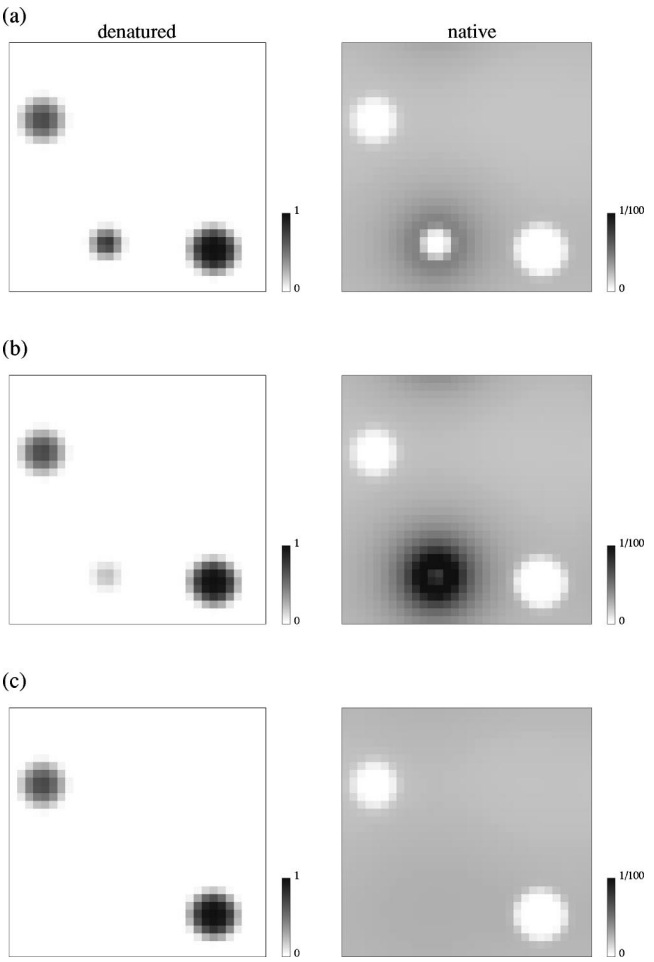

FIG. 4. Cross section of the density fields of the native (right panels) and denatured (left panels) proteins. Times: (a) $t = 1.06 \times 10^5$, (b) $t = 1.07 \times 10^5$, (c) $t = 1.08 \times 10^5$. Note that the gray scale ranges from 0 to 1 in the left panels (denatured), and from 0 to 0.01 in the right panels (native).

We first study the case of the nucleationlike regime. All the parameters except for ρ_C are the same as those given in the previous section: $\epsilon_{D,D} = -0.11$, $\rho_P = 0.1$, $R_N = R_C = 0.4$, and $R_D = 0.6$. Simulations with different values of ρ_C were performed. The morphological behavior was found to be essentially the same as depicted in Figs. 1(a)–1(c) as long as aggregation occurred. The time evolution of some physical quantities is shown in Fig. 5.

As is apparent from this figure, aggregation does not take place for $\rho_C = 0.4$ or 0.8 (Fig. 5), and the simulations resulted in a completely uniform phase, which is indicated by the value of spatial deviation s_N nearly equal to zero [Fig. 5(d)]. The uniformity of the system is also reflected in the sharp drop in $2\pi/\langle k \rangle$ for $\rho_C = 0.4$ and 0.8 [Fig. 5(a)]: since the mode $\mathbf{k} = \mathbf{0}$ is not included in the definition of $\langle k \rangle$ [Eq. (25)], only meaningless small modes are apparently left when modes converge to $\mathbf{k} = \mathbf{0}$, that is, when the system becomes completely uniform. It should be emphasized that the param-

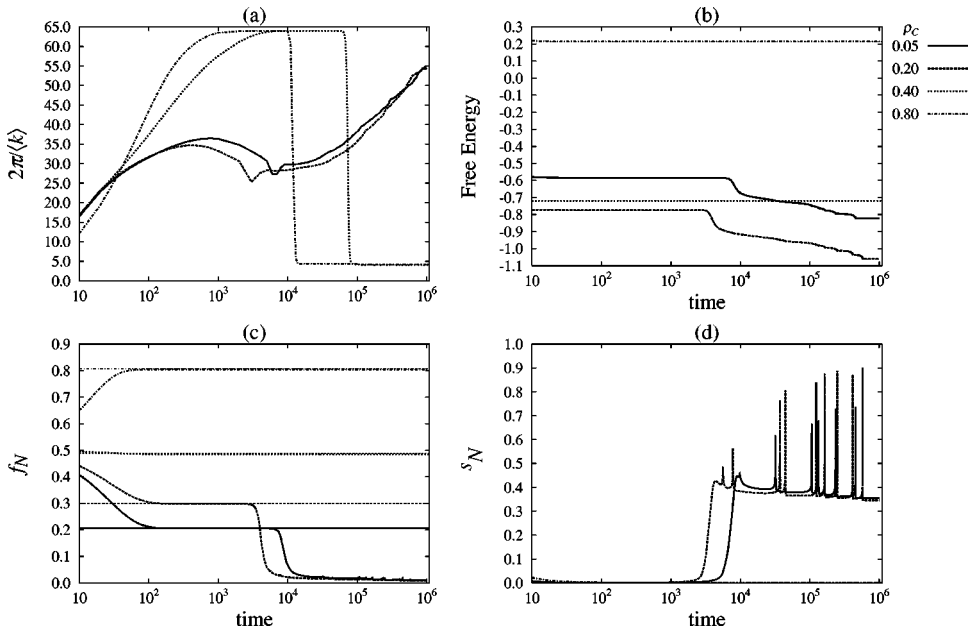

FIG. 5. Time evolution of physical quantities with $\epsilon_{D,D}=-0.11$ (nucleationlike regime). Horizontal narrow lines in (c) are the equilibrium values of f_N in the uniform system. Only one out of ten trajectories is shown in (b), (c), and (d) for each set of simulations.

eter set in all the cases here corresponds to the aggregation phase at equilibrium [13] although aggregation was not observed in the present dynamics simulations for $\rho_C=0.4$ and 0.8. Therefore, aggregation is kinetically inhibited. In these cases, the final values of f_N are the same as the one obtained from equilibrium calculations for the uniform system.

For $\rho_C=0.05$ and 0.2 (Fig. 5), aggregation takes place. The time evolution of the native fraction f_N shows that in the quasiuniform phase before the onset of aggregation the native protein is more stabilized in the case of $\rho_C=0.2$ than in the case of $\rho_C=0.05$. In addition, the onset of aggregation is earlier for $\rho_C=0.2$ than for $\rho_C=0.05$. A phase diagram presented in our previous paper [13] showed that, as ρ_C increases, the aggregation of the denatured proteins is more enhanced while the native protein is more stabilized as long as the system is uniform (i.e., when aggregation does not occur). Therefore, the time evolution of f_N for $\rho_C=0.05$ and 0.2 in Fig. 5(c) exhibits crowding effects analogous to those at equilibrium, that is, in the aggregation process, as ρ_C increases, the onset of aggregation of the denatured protein is accelerated while the native protein is more stabilized in the quasiuniform phase before aggregation. It is observed that the values of f_N at their plateau are almost identical to those at equilibrium in the uniform phase [Fig. 5(c)]. In the time range between $t\sim10^4$ and $\sim5\times10^5$, the growth of aggregates seems faster for $\rho_C=0.05$ than for $\rho_C=0.2$ [Fig. 5(a)]. There are two possible reasons for this observation. First, it is expected that the effective diffusion rate is slower in the more crowded system so that the diffusion of proteins from vanishing aggregates and/or dissolved regions into growing aggregates becomes slower. Second, the presence of more crowding agents increasingly stabilizes all the aggregates so that disappearance of smaller aggregates is hindered. The latter point is supported by our previous results for the crowded system at equilibrium where it was shown that the aggregation of the denatured protein is enhanced as the crowding agent density is increased [13].

The difference becomes indistinguishable after $t\sim5\times10^5$ because, in this time range, there is usually only one aggregate in the system so that the aggregation process is essentially finished and the final aggregate simply rearranges itself to become more spherical. For higher values of ρ_C ($=0.4$ or 0.8), the native protein is so highly stabilized in the quasiuniform phase before aggregation that the number of the denatured proteins is not large enough to form nuclei of aggregates; hence the system is trapped in a uniform state which is metastable.

Next we examined the spinodal decomposition regime of aggregation ($\epsilon_{D,D}=-0.2$) In this case, the aggregation of the denatured protein was observed for all the studied values of $\rho_C=0.05$, 0.2, 0.4, and 0.8 (not shown). Since aggregation is not usually observed in the living cell, the spinodal decomposition regime should be biologically less relevant than the nucleationlike regime. Therefore, hereafter we focus our attention to the latter.

C. Crowding effects on folding, unfolding, and aggregation

We now turn to the crowding effects on protein folding, unfolding, and aggregation. As noted above, we limit our investigation to the nucleationlike regime in this section.

In order to simulate folding and unfolding processes, two different initial conditions were used. As the initial condition for simulating folding process, we set $\phi^N(\mathbf{r})=0.001\rho_P[1+\xi^N(\mathbf{r})]$, $\phi^D(\mathbf{r})=0.999\rho_P[1+\xi^D(\mathbf{r})]$, and $\phi^C(\mathbf{r})=\rho_C[1+\xi^C(\mathbf{r})]$, where $\xi^\alpha(\mathbf{r})$ are uniform random fields in the range $[-0.1,0.1]$. This choice represents a situation in which the proteins are mostly denatured at the beginning of the simulation; hence we call such a simulation an ''initially denatured simulation.'' On the other hand, the initial condition for simulating the unfolding process is such that the proteins are mostly in their native state initially, namely, $\phi^N(\mathbf{r})=0.999\rho_P[1+\xi^N(\mathbf{r})]$, $\phi^D(\mathbf{r})=0.001\rho_P[1+\xi^D(\mathbf{r})]$, and the crowding agent density field is the same as above. We call

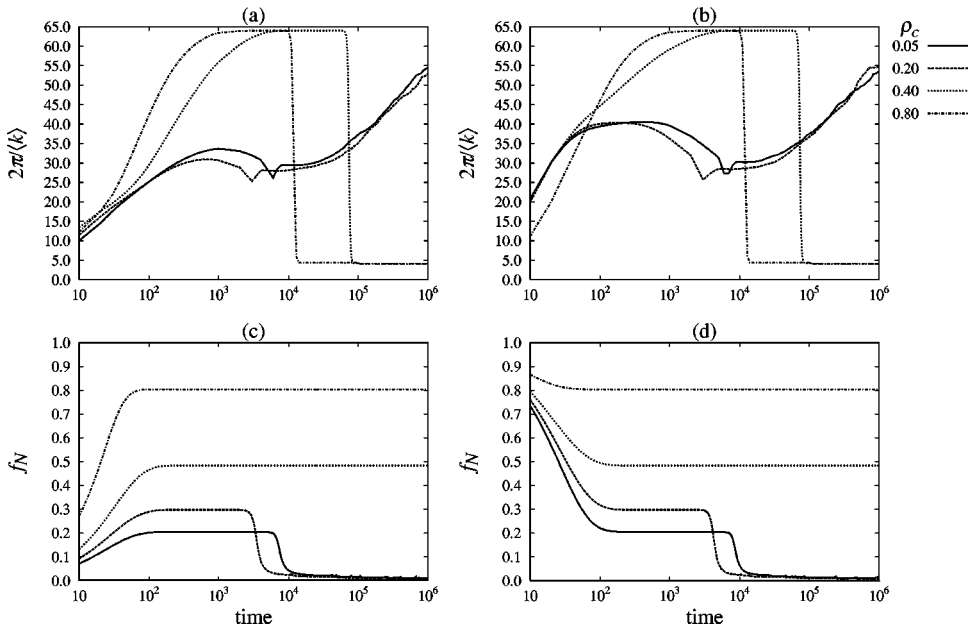

FIG. 6. Time evolution of characteristic length (a) and (b); fraction of the native protein (c) and (d). (a) and (c) correspond to ''initially denatured simulations,'' and (b) and (d) to ''initially native simulations'' with $\eta_{TS}=1$.

the simulation with such an initial condition the ''initially native simulation.''

The first set of simulations was performed with the same choice of parameters as in the previous sections: $\epsilon_{D,D}=-0.11$, $\rho_P=0.1$, $R_N=R_C=0.4$, and $R_D=0.6$. We also note that the intrinsic free energy of the transition state protein is set as $\eta_{TS}=1$ in this case so the activation free energies of folding and unfolding in the dilute solution, $\eta_{TS}-\eta_D$ and $\eta_{TS}-\eta_N$, are both equal to unity. The results of the simulations with different values of the bulk crowding agent density ρ_C are shown in Fig. 6.

In both cases of initially denatured and initially native simulations, aggregation of the denatured protein occurs for $\rho_C=0.05$ and 0.2 but not for higher values of ρ_C ($=0.4$ and 0.8). In other words, whether or not the aggregation occurs is independent of the initial fraction of the native protein in the present case. For the cases in which the aggregation occurs ($\rho_C=0.05$ and 0.2), the characteristic length becomes larger in the initially native simulations than in the initially denatured ones before the onset of the aggregation [Figs. 6(a) and 6(b)]. For the cases in which the aggregation does not occur ($\rho_C=0.4$ and 0.8), the rate of folding is faster for more crowded solutions [Fig. 6(c)]. However, as soon as the initial plateau in the fraction of the native protein f_N is reached, the time evolution of the characteristic length f_N and the relative spatial deviation of the native protein field s_N in later stages all show almost the identical behavior in the initially denatured [Figs. 6(a) and 6(c)] and initially native [Figs. 6(b) and 6(d)] simulations; namely, they are the same as presented in the previous section.

Next we examine the case in which the protein folds and unfolds more slowly. This case is simulated with the intrinsic free energy of the transition state protein $\eta_{TS}=5$ so that the activation free energies of folding and unfolding in the dilute solution are as high as 5 unit energy. Other parameters are the same as in the previous paragraph. These simulations exhibit qualitatively different behaviors depending on the initial fraction of the native protein (Fig. 7).

When the proteins are mostly denatured initially (initially denatured simulations), aggregation of the denatured protein occurs for all the values of ρ_C ($=0.05$, 0.2, 0.4, and 0.8), and the onset of aggregation is earlier in more crowded solutions. However, when the proteins are mostly native initially (initially native simulations), the aggregation does not occur for high values of ρ_C ($=0.4$ and 0.8). Furthermore, for the cases in which the aggregation occurs in both initially native and initially denatured simulations ($\rho_C=0.05$ and 0.2), the onset of aggregation is much earlier and the plateau in f_N before the onset is not observed in the initially denatured case. The time evolution of the characteristic length for the initially native simulations with $\rho_C=0.05$ and 0.2 indicates that the system becomes almost completely uniform before the onset of aggregation, but so is not the case in the initially denatured simulations in which the characteristic length exhibits only a minor increase before the onset of the aggregation. To summarize, compared to the proteins with low folding and unfolding activation free energies ($\eta_{TS}-\eta_D=\eta_{TS}-\eta_N=1$), the ones with high activation free energies ($\eta_{TS}-\eta_D=\eta_{TS}-\eta_N=5$) are more prone to aggregation when the proteins are initially denatured, and whether or not aggregation occurs depends on the initial conditions. Figure 7 also suggests that the aggregation of slow-folding proteins may be suppressed in highly crowded conditions once most of the proteins have reached the native state.

IV. DISCUSSION

The present simulations revealed morphological variations in the process of aggregation of denatured proteins. However, as far as we are aware at present, there is no experimental works on the morphological evolution of the aggregates of denatured proteins. Yong *et al.* [23] used small angle neutron scattering to study the intermediate structure of amyloid fibril assembly. The same technique or light scattering [24] should be applicable to study the structure of the denatured protein aggregates.

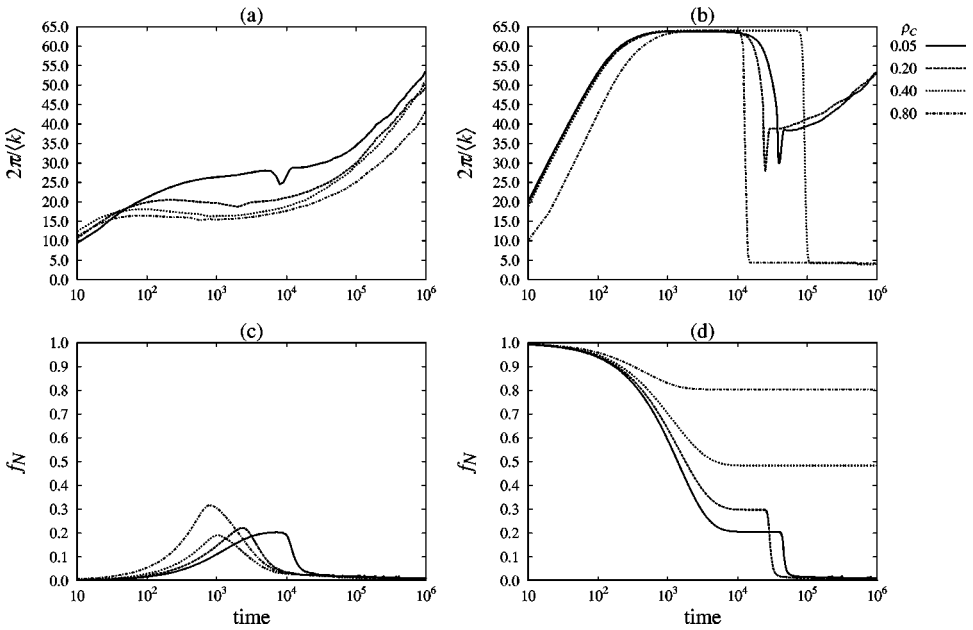

FIG. 7. Time evolution of characteristic length (a) and (b); fraction of the native protein (c) and (d). (a) and (c) correspond to initially denatured simulations, and (b) and (d) to initially native simulations with $\eta_{TS}=5$.

Our simulations suggest that macromolecular crowding effects on aggregation (when it occurs) can be classified into three categories, namely, (i) stabilization of the native protein before the onset of aggregation, (ii) acceleration of the onset of aggregation and growth of aggregates at early stages, and (iii) deceleration of the equilibrating process of aggregation at later stages. These three types of crowding effect observed in both the nucleationlike and spinodal decomposition regimes, and become more conspicuous for more crowded solutions. We have shown in our previous paper [13] that, as the bulk density of the crowding agent increases, the native protein is stabilized unless aggregation occurs, and aggregation of the denatured protein is enhanced. Therefore, the crowding effects (i) and (ii) above are analogous to those at equilibrium. The experimental observation that crowding accelerates amyloid formation [8] partly supports the simulation results (ii). Experimental validation of the stabilization effect of crowding (i) listed above will require time-resolved techniques since the latent time before the onset of aggregation may be short.

For large values of the bulk density of crowding agent ρ_C ($=0.4$ or 0.8) in the nucleationlike regime, aggregation is inhibited and the system becomes uniform in which a substantial fraction of the native proteins is dissolved (Fig. 5). In reality, this inhibition of aggregation by the crowding agent is not indefinite since thermal fluctuation will sometimes cause the formation of nuclei of aggregates some of which may grow to a macroscopic extent. In our present model, however, no thermal fluctuation (random noise) is included in the diffusion-reaction equations (9); hence aggregation cannot occur once the system becomes uniform. Inclusion of random noise terms representing thermal fluctuation is left for future studies. Nevertheless, the present results and previous ones [13] suggest that macromolecular crowding may help to kinetically prevent aggregation of denatured proteins inside the living cell despite the fact that the aggregation is more favored at equilibrium.

The simulations with initially native and initially denatured proteins indicate that crowding accelerates the rate of folding for fast-folding proteins as well as the onset of aggregation for slow-folding proteins. These results can be compared to the experimental results of van den Berg *et al.* [25,26] who studied folding of oxidized and reduced hen lysozyme in varying concentrations of crowding agents. The folding rate of the reduced lysozyme is known to be smaller than that of the oxidized lysozyme. van den Berg *et al.* found that the folding rate of the oxidized lysozyme is significantly increased while that of the reduced lysozyme is retarded in the presence of a high concentration of crowding agents such as bovine serum albumin and Ficoll [26]. They have also shown in another experiment that folding of the reduced lysozyme is severely disturbed by crowding agents, resulting in irreversible aggregation of non-native structures, while the folding yield of the oxidized lysozyme was essentially unaffected [25]. Some of these experimental observations are in good accordance with the present dynamics simulations. That is, the folding rate of fast-folding proteins becomes faster in more crowded solutions [Fig. 6(c)], while folding of slow-folding proteins is disturbed, resulting in aggregation [Fig. 7(c)]. However, the folding yield of fast-folding proteins in the present simulation increases in more crowded solutions [Fig. 6(c)], which is not consistent with the experiment. (Note that the experiments of van den Berg *et al.* [25,26] were also discussed in terms of the size dependence of the crowding effect in our previous paper [13].) The difference between fast- and slow-folding proteins regarding the tendency for aggregation has an important implication in biological contexts, that is, fast-folding proteins are less liable to aggregation so that even if they are denatured at one time they can rapidly refold to the native state and avoid quasi-irreversible aggregation.

Recently, molecular simulation studies have been performed to investigate the competition between protein folding and aggregation [10–12]. These simulations with detailed description of protein molecules have revealed the sensitivity of the native and aggregate conformations to

amino acid sequences [10,12]. However, no simulation has been performed so far to study macromolecular crowding effects on protein folding and aggregation. Klimov *et al.* [27] carried out molecular simulations of folding of a single protein chain (a β-hairpin peptide) confined inside a spherical pore. Molecular confinement imposes effects similar to macromolecular crowding [4]. Klimov *et al.* [27] found that molecular confinement generally accelerates the folding of the β-hairpin formation, and that this acceleration is not monotonic with respect to the radius of the spherical pore but has a maximum value at the radius of the sphere that is 50% larger than that of the folded β-hairpin peptide. They also report that the denatured state ensemble in the confined system was significantly different from that in the bulk system [27]. Therefore, the present density functional simulations are in qualitative agreement regarding the acceleration effect of crowding or confinement, but the results of the molecular simulations suggest that it is important to take into account protein chain conformations explicitly. In the present theoretical framework, all the molecules are assumed to be spherical with fixed sizes; hence the conformational changes of the denatured protein due to crowding are not treated. However, it is possible to include such conformational changes in the present theory. A trivial possibility is to assume multiple conformational species with different sizes for the ensemble of denatured proteins, as was done by Minton [28] in his statistical thermodynamic theory of crowding effects on protein stability. Another possible way is to treat chain conformations explicitly as is done in density functional simulations of polymer melts [15,16], although this extension may be complicated because of the uniqueness of the native conformation. Nevertheless, the present density functional approach will serve to investigate mesoscopic to macroscopic behaviors of protein aggregation and macromolecular crowding which can well complement microscopic molecular simulation studies.

V. CONCLUSION

We presented a dynamic density functional theory which describes a system consisting of proteins and macromolecules. The results of dynamics simulations are qualitatively in good agreement with experimental observations regarding acceleration of aggregation, acceleration of folding for fast-folding proteins, and disturbed folding of slow-folding proteins. A dynamic stabilization effect by crowding was also observed. The present theory, with possible calibration of interaction parameters, may provide insights into the properties and behaviors of proteins inside the living cell.

[1] A.B. Fulton, Cell **30**, 345 (1982).
[2] S.B. Zimmerman and A.P. Minton, Annu. Rev. Biophys. Biomol. Struct. **22**, 27 (1993).
[3] A.P. Minton, Curr. Opin. Struct. Biol. **10**, 34 (2000).
[4] A.P. Minton, J. Biol. Chem. **276**, 10577 (2001).
[5] R.J. Ellis, Curr. Opin. Struct. Biol. **11**, 114 (2001).
[6] R.J. Ellis, Trends Biochem. Sci. **26**, 597 (2001).
[7] M. Bucciantini, E. Giannoni, F. Chiti, F. Baroni, L. Formigli, J. Zurdo, N. Taddei, G. Ramponi, C.M. Dobson, and M. Stefani, Nature (London) **416**, 507 (2002).
[8] D.M. Hatters, A.P. Minton, and G.J. Howlett, J. Biol. Chem. **277**, 7824 (2002).
[9] A.P. Minton, Methods Enzymol. **295**, 127 (1998).
[10] P.M. Harrison, H.S. Chan, S.B. Prusiner, and F.E. Cohen, J. Mol. Biol. **286**, 593 (1999).
[11] A.V. Smith and C.K. Hall, J. Mol. Biol. **312**, 187 (2001).
[12] R.I. Dima and D. Thirumalai, Protein Sci. **11**, 1036 (2002).
[13] A.R. Kinjo and S. Takada, Phys. Rev. E **66**, 031911 (2002).
[14] K. Kawasaki, *Non-Equilibrium and Phase Transition* (Asakura Shoten, Tokyo, 2000) (in Japanese).
[15] T. Kawakatsu, *Foundations of Polymer Physics* (Saiensu Sha, Tokyo, 2001) (in Japanese).
[16] J.G.E.M. Fraaije, B.A.C. van Vlimmeren, N.M. Maurits, M. Postma, O.A. Evers, C. Hoffmann, P. Altevogt, and G. Goldbeck-Wood, J. Chem. Phys. **106**, 4260 (1997).
[17] L.D. Landau and I.M. Lifshitz, *Statistical Physics, Part I*, 3rd ed. (Iwanami Shoten, Tokyo, 1980) (Japanese translation).
[18] A. Fersht, *Structure and Mechanism in Protein Science* (Freeman, New York, 1999).
[19] B.A.C. van Vlimmeren and J.G.E.M. Fraaije, Comput. Phys. Commun. **99**, 21 (1996).
[20] J.F. Gouyet, Phys. Rev. E **51**, 1695 (1995).
[21] A. Abdulle and A.A. Medovikov, Numer. Math. **90**, 1 (2001).
[22] A. Shinozaki and Y. Oono, Phys. Rev. E **48**, 2622 (1993).
[23] W. Yong, A. Lomakin, M.D. Kirkitadze, D.B. Teplow, S.H. Chen, and G.B. Benedek, Proc. Natl. Acad. Sci. U.S.A. **99**, 150 (2002).
[24] T.G. Parker and D.G. Dalgleish, Biopolymers **16**, 2533 (1977).
[25] B. van den Berg, R.J. Ellis, and C.M. Dobson, EMBO J. **18**, 6927 (1999).
[26] B. van den Berg, R. Wain, C.M. Dobson, and R.J. Ellis, EMBO J. **19**, 3870 (2000).
[27] D.K. Klimov, D. Newfield, and D. Thirumalai, Proc. Natl. Acad. Sci. U.S.A. **99**, 8019 (2002).
[28] A.P. Minton, Biophys. J. **78**, 101 (2000).